



Article

Benchmark Angle-Differential Cross-Section Ratios for Excitation of the 4p⁵5s Configuration in Krypton

Ahmad Sakaamini ¹, Jean-Baptiste Faure ¹, Murtadha A. Khakoo ^{1,*}, Oleg I. Zatsarinny ^{2,†} and Klaus Bartschat ²

- Department of Physics, California State University, Fullerton, CA 92831, USA; asakaamini@Fullerton.edu (A.S.); jfaure@fullerton.edu (J.-B.F.)
- Department of Physics and Astronomy, Drake University, Des Moines, IA 50311, USA; klaus.bartschat@drake.edu
- * Correspondence: mkhakoo@fullerton.edu
- † Deceased.

Abstract: Benchmark intensity ratio measurements of the energy loss lines of krypton for excitation of the $4p^6$ $^1S_0 \rightarrow 4p^55s[3/2]_2$, $4p^55s[3/2]_1$, $4p^55s'[1/2]_0$, and $4p^55s'[1/2]_1$ transitions are reported, these being the lowest electronic excitations for krypton. The importance of these ratios as stringent tests of theoretical electron scattering models for the noble gases is discussed, as well as the role of spin-exchange and direct processes regarding the angular dependence of these ratios. The experimental data are compared with predictions from fully-relativistic *B*-spline *R*-matrix (close-coupling) calculations.

Keywords: electron scattering; excitation; krypton; angle-differential cross-section ratios; close-coupling; Dirac B-spline R-matrix



Citation: Sakaamini, A.; Faure, J.-B.; Khakoo, M.A.; Zatsarinny, O.I.; Bartschat, K. Benchmark Angle-Differential Cross-Section Ratios for Excitation of the 4p5s Configuration in Krypton. *Atoms* 2021, 9, 61. https://doi.org/ 10.3390/atoms9030061

Academic Editor: Emmanouil P. Benis

Received: 10 August 2021 Accepted: 29 August 2021 Published: 2 September 2021

Publisher's Note: MDPI stays neutral with regard to jurisdictional claims in published maps and institutional affiliations.



Copyright: © 2021 by the authors. Licensee MDPI, Basel, Switzerland. This article is an open access article distributed under the terms and conditions of the Creative Commons Attribution (CC BY) license (https://creativecommons.org/licenses/by/4.0/).

1. Introduction

The heavy rare gases are of great interest in both industry and collision physics. There is a wide array of applications involving the use of species such as krypton and xenon, with the most popular being that they act as excellent buffers in plasmas. Krypton is found primarily in the Earth's atmosphere. It is widely used in electron impact-initiated plasmas for fluorescent lighting [1], flash lamps for use in high-speed photography [2], and high-power gas lasers [3]. In fundamental physics, species such as krypton are excellent candidates for studies in spectroscopy, primarily because of their rich target structure involving spin-exchange and relativistic effects such as spin-orbit coupling, which are important in both the target structure and the scattering continuum [4].

A comprehensive theoretical study of electron scattering for the noble gases Ne, Ar, Kr, and Xe based on the semi-relativistic distorted-wave method was reported by Bartschat and Madison [5]. Exchange effects were approximated by the semi-empirical local model potential suggested by Furness and McCarthy [6], while relativistic effects were accounted for through the one-electron spin-orbit term of the Breit-Pauli Hamiltonian. These potentials were added to the static Hartree potential generated from the final-state electronic configuration of the target, and the distorted waves were then calculated in that potential. A few years later, Zuo et al. [7] developed a fully relativistic distorted-wave approximation (RDWA), yielding results of comparable accuracy relative to those obtained by Bartschat and Madison. In both models, the $(np^6)^1S_0$ ground state and the $np^5(n+1)s$ excited states were described by single-configuration states. Note that the two excited states with total electronic angular momenta J = 0.2 are actually well LS-coupled, while the two I=1 states are a linear combination of two states, with the details depending on the coupling scheme used. Bartschat and Madison, for example, adopted the so-called "intermediate coupling scheme" in which a linear combination of LS-coupled $^1\mathrm{P}_1$ and $^3\mathrm{P}_1$ state is used.

Atoms 2021, 9, 61 2 of 14

Table 1 shows the result of a multi-configuration expansion of the states of interest for the present work. The Cowan code [8] only uses one term-averaged 5s orbital. One can clearly observe that a single configuration dominates in all cases, and also that the two J=1 states are essentially a 50/50 mix of states with singlet and triplet spin character.

Table 1. Intermediate-coupling coefficients for the $4p^6$ and $4p^5$ 5s states of Kr in a multi-configuration expansion, produced with the Cowan code [8] by Fontes [9]. E_L values from the Cowan code and from Moore [10] are also listed. The notation $[K]_J$ (see also below) indicates the total electronic angular momentum of the $(4p^5)^2P_K$ ionic core. After coupling to the outer orbital (here 5s), this results in the total electronic angular momentum J of the state. Refer to the text for discussions.

T1 #	Canfianation	Intermediate Counting	E_L (eV)
Level #	Configuration	Intermediate Coupling	Cowan	Moore
1	4p ⁶	$0.998 (4p^6)^1S_0$	0.00	0.00
2	$4p^55s[3/2]_2$	$0.998 (4p^{5}5s)^{3}P_{2}$	9.88	9.92
3	$4p^55s[3/2]_1$	$0.67 (4p^55s)^3P_1 + 0.74 (4p^55s)^1P_1$	9.97	10.03
4	$4p^55s[1/2]_0$	$0.996 (4p^55s)^3P_0$	10.50	10.56
5	$4p^55s[1/2]_1$	$0.74(4p^55s)^3P_1 - 0.67(4p^55s)^1P_1$	10.56	10.64

A major breakthrough in the treatment of electron–atom collision came in the 1990s with the convergent close-coupling (CCC) [11,12] and *R*-matrix (close-coupling) with pseudostates (RMPS) [13,14] methods. The general idea is the same, namely to extend the traditional low-energy close-coupling method to intermediate and even high energies by introducing so-called pseudo states. These have the mathematical properties of bound states (most importantly, they are easily normalizable), but due to their confinement to either a hard (*R*-matrix) or soft (CCC with a Laguerre basis) box, they provide a discretization of the target continuum. While these methods have been very successful for light (quasi-)one-electron and (quasi-)two-electron atomic and ionic targets, even the H₂ molecule [15], the situation is much less satisfactory for more complex, open-shell targets, especially if these targets are also heavy; hence, both electron correlation and relativistic effects need to be described properly by the theoretical approaches.

Concerning the heavy noble gases in particular, this is a situation where the targets are convenient for experimental investigations but difficult for theory. Numerous high-quality experimental datasets have existed already for a while (see, for example, refs. [16–19] from our own group as just a small selection), but comparisons with those data have been rare due to the challenges faced by theory. The currently available version of the CCC code remains limited to one-electron and two-electron systems outside of a structureless $^{1}S_{0}$ core. The well-known R-matrix code of the Belfast group [20] has been extended to the RMPS framework, but applications to the heavy noble gases using the full power of the approach have also been limited—likely due to the fact that the target description with strongly term-dependent one-electron valence orbitals remains a challenge, although sufficiently large configuration interaction (CI) expansions should be able to solve this problem even if all one-electron orbitals are forced to be orthogonal to each other.

A very promising method available for these targets is the *B*-spline *R*-matrix (BSR) approach that allows the use of non-orthogonal sets of one-electron orbitals and employs *B*-splines to represent them. Technically, this has the advantages of compact CI expansions yielding sufficient accuracy as well as accurate and efficient integration schemes. A general computer code that can be used for calculations of atomic structure, photo-ionization, and electron collisions in a non-relativistic and semi-relativistic (Breit–Pauli) framework was published by Zatsarinny [21] and used for numerous calculations of the above processes. A review of the method and its applications until 2013 was published by Zatsarinny and Bartschat [22]. Similarly to the Belfast code, the available suite of computer codes is *general*, i.e., it is applicable to targets such as the heavy noble gases of interest for the present work. A fully-relativistic version described by Zatsarinny and Bartschat [23] also

Atoms 2021, 9, 61 3 of 14

exists. While a comprehensive write-up is not available due to the untimely death of Dr. Zatsarinny in March 2021, the code with instructions is freely available on his GitHub site [24].

2. Cross-Section Ratios

Disagreements observed between the theory and experiment, even for angle-integrated cross sections, are often accredited to the challenges faced in the absolute normalization of the experimental data using conventional electrostatic electron spectrometers [25]. This problem has been difficult to overcome systematically when normalizing inelastic scattering features, with non-zero energy loss E_L , to the elastic scattering feature ($E_L = 0$) as a standard. This is due to the required accurate characterization of the spectrometer analyzer's detection efficiency for different E_L values in the spectrum. Therefore, in order to obtain absolute inelastic differential cross sections (DCS), the scattering intensity of inelastic features in the same energy loss spectrum is normalised to the elastic scattering intensity by using DCSs for elastic scattering at the same incident electron energy (E_0) and scattering angle θ , assuming that the detection efficiency across the electron energy loss spectrum is accurately known. Elastic scattering DCSs can be accurately determined by using the standard relative flow method [26] and can be used as a calibration in the observed electron energy loss spectra. However, the added problem to determine accurately normalized inelastic DCSs suffers, as aforesaid, from the accurate determination of the detection efficiency of the scattered electron detector across the observed energy loss spectrum, i.e., as a function of the residual energy of the scattered electron energy E_R (= $E_0 - E_L$). Knowing this, the absolute inelastic DCSs may be determined from the spectrum if the elastic DCS is known in tandem with the analyzer detection efficiency. This is indeed the case for time-of-flight electron spectrometers, where the detection efficiency is independent of E_R of the scattered electron.

At CSUF, we recently built an electron time-of-flight (TOF) spectrometer to determine accurate elastic-to-inelastic differential electron scattering ratios for the excitation of the $X^1\Sigma_q^+ \to b^3\Sigma_u^+$ transition in H₂. These benchmark ratios were found to be in excellent agreement with the CCC predictions of the Curtin University group [27]. After normalizing our TOF spectrum's elastic feature to corresponding well-established elastic electron scattering DCSs from our group [28], these resulted, in turn, in benchmark theoretical and experimental DCSs for elastic and inelastic processes for the H₂ molecule. Since it is much easier and more reliable to measure relative ratios in scattering experiments, we decided to revisit inelastic scattering ratios for the lowest transitions in Kr to provide further experimental benchmark data for testing existing and future collision models. Such ratio measurements were earlier carried out by us for Ne [29], Kr [18,19], and Xe [16]. DWBA calculations for these ratios, particularly regarding the observed deviations from statistical ratios, were also reported by Bartschat and Madison [30]. Referring to the excellent agreement between the experimental ratios of [29] and the predictions from their semi-relativistic BSR calculations for Ne, Zatsarinny and Bartschat [31] recommended such relative inelastic scattering ratios in the heavy noble gases as representing "a very sensitive test to the quality of the theoretical model".

The present work with a Kr target focuses on inelastic scattering ratios only in order to draw attention to such ratios as benchmarks to aid theory in a critical area of experimental and theoretical electron collision physics. DCS ratios have been determined for the first four excitation levels. We define these ratios as follows.

$$r(E_0, \theta) = \frac{I_1(E_0, \theta)}{I_3(E_0, \theta)} \equiv \frac{\sigma(5s[3/2]_2)}{\sigma(5s'[1/2]_0)},$$
(1)

$$r'(E_0, \theta) = \frac{I_2(E_0, \theta)}{I_4(E_0, \theta)} \equiv \frac{\sigma(5s[3/2]_1)}{\sigma(5s'[1/2]_1)},$$
(2)

$$r''(E_0, \theta) = \frac{I_1(E_0, \theta)}{I_2(E_0, \theta)} \equiv \frac{\sigma(5s[3/2]_2)}{\sigma(5s[3/2]_1)},\tag{3}$$

Atoms 2021, 9, 61 4 of 14

$$r'''(E_0, \theta) = \frac{I_3(E_0, \theta)}{I_4(E_0, \theta)} \equiv \frac{\sigma(5s'[1/2]_0)}{\sigma(5s'[1/2]_1)}.$$
 (4)

Here, $I_m(E_0,\theta)$ (m=1-4, see labels in Figure 1) are the intensities of the electron energy loss features for excitation of the $4p^6 \rightarrow 4p^55s$, $5s'[K]_J$ transition, which are proportional to the differential cross section σ . In our notation and discussion below, we use the intermediate-coupling scheme [8,29] that is appropriate for the heavy noble gases in which K is the total angular momentum of the parent ion $4p^5$ core and J is the total angular momentum of the core plus valence 5s, 5s' electron. The ratio r defined in Equation (1) addresses the ratio between the pure triplet $5s[3/2]_2$ (3P_2) and $5s'[1/2]_0$ (3P_0) states (with its approximate LS-coupled component in brackets), respectively. Since the statistical weights are 2J+1, one would expect the DCS ratio to be close to five for a well LS-coupled system, provided one can neglect the energy difference between the two states as well as the potential term dependence of the valence orbital. In order to indicate those possible effects, we follow the standard notation of using 5s and 5s' for the outer orbital when the parent ion is either the $(4p^5)^2P_{3/2}$ (for 5s) or the $(4p^5)^2P_{3/2}$ (for 5s') state.

On the other hand, the observable r' defined in Equation (2) addresses the ratio for the $5s[3/2]_1$ and $5s'[1/2]_1$ states. While the appropriate intermediate-coupling coefficients can be deduced from the respective line strengths if these two J=1 states are written as a linear combination of LS-coupled 1P_1 and 3P_1 states [5], the ratio r' can be used as a test of how well a collision model accounts for the respective excitation portions as well as the interference of the singlet and triplet contributions [29]. At sufficiently high energies and small angles, one would expect $r' \approx a^2/b^2$, where a and b are the coefficients of the 1P_1 term in the intermediate-coupling description of the two states [30]. In the present case (see Table 1), this would suggest an asymptotic ratio of $r' \approx 1.2$.

Next, r'' defined in Equation (3) represents the ratio of the LS-coupled $5s[3/2]_2$ (3P_2) state and the mixed-coupled $5s[3/2]_1$ state, while r''' defined in Equation (4), in a similar fashion as r'', is the ratio between the pure $\sigma(5s'[1/2]_0$ (3P_0) state and the other mixed state, $(5s'[1/2]_1)$. From an experimental point of view, it is important to note that r'' and r''' are less affected by the instrumental transmission efficiency than r and r', since the features in r'' and r''' are very closely spaced in energy loss. This is especially important at low E_0 values close to threshold and will be further addressed in the following experimental section.

In this paper, the recently obtained inelastic DCS ratios for Kr are presented in comparison with the respective theoretical predictions, as well as the earlier experimental ratios obtained in our group by Guo et al. [4]. A brief summary of the fully relativistic D(irac)BSR electron scattering model for Kr is given in the next section. More details, also including the Xe target, can be found in [32]. This is followed by a discussion of the experimental apparatus and the measurement procedures for obtaining the above-mentioned DCS. The experimental and theoretical results are presented and discussed in detail in Section 5 before we finish with a summary and our conclusions in Section 6.

3. Theory

Since the details of the calculation were given by Zatsarinny and Bartschat [32], we only summarize the main points here. The calculations reported in this paper were performed using the R-matrix (close-coupling) approach, as implemented in the DBSR suites of computer codes. The initial structure calculation for Kr^+ was carried out with the GRASP2K relativistic atomic-structure package [33]. After that, the valence orbitals were generated in a frozen-core calculation for Kr^+ by using the average-term approximation. All these states of Kr^+ were then used as target states in B-spline bound-state close-coupling calculations in order to generate the low-lying states of atomic Kr (with N=36 electrons) employing non-orthogonal, term-dependent orbitals for each Kr state.

In the scattering calculations, we included the lowest 31 physical states of Kr, i.e., the fine-structure levels with configurations 4p⁵5s, 4p⁵5p, 4p⁵4d, and 4p⁵6s, respectively. This model will be referred to as DBSR-31 below. Since this is a fully-relativistic approach, the mixing coefficients in the multi-configuration expansions are mathematically not the

Atoms 2021, 9, 61 5 of 14

same as in the intermediate-coupling scheme. This is a similar situation as in the RDW model [7]. In a truly complete expansion, the specifics of the numerical basis would not matter. While this ideal situation is not achievable in practice, it still makes some sense to interpret the final results in the intermediate-coupling scheme, which appears to capture the essential physics regarding the orbital and spin angular momentum character of the states in question.

We then used the DBSR version [23] to solve the (N+1) electron collision problem. We calculated partial-wave contributions up to J=61/2 numerically. No extrapolation scheme to account for even higher partial waves was necessary for all observables presented in this paper.

At this time, the only results from the 31-state model are available. In the original paper [32], 47 state results were also presented, but both calculations were limited to energies below 13.5 eV. Note that the general features seen in the near-threshold region were reproduced in both models (except very close to threshold, where there are no experimental data for the ratios), although the absolute values differed. In the comparison with experiment, the available data were visually normalized to the 47 state results, which made the latter calculation appear more superior. Since we compare ratios in the present paper, the 31 state model should be reasonable. Ideally, one would extend these calculations much further to include a large number of pseudo-states to also couple to the ionization continuum. Due to the passing of Dr. Zatsarinny, however, this is not realistic in the timeframe for this Special Issue dedicated to him.

4. Experiment

The present California State University (CSUF) energy loss system is a moderate-current, high-resolution electrostatic energy loss spectrometer, which has been well tested and described in detail before [34]. The system consists of an electron monochromator and an electron energy analyzer, with both employing hemispherical energy selectors. The collimated gas beam is delivered to the collision region via a moveable gas aperture source, which is aligned and placed about 5 mm below the collision region. The entire spectrometer is housed in a vacuum chamber that is pumped with a 12 inch diffusion pump down to a base pressure of $\approx 1\times 10^{-7}$ Torr. In order to create and maintain an environment suitable for measuring stable low-energy electron energy loss spectra over long periods of time, the electron gun and energy analyzer are both baked to about $\approx 120\,^{\circ}\text{C}$ during the experiment, and the vacuum chamber is properly oil-baffled.

The experimental apparatus is computer controlled via a LabVIEW program that is run in the multi-channel scaling mode and monitors the input pressure of the target gas, steers the moveable gas source in and out of the interaction region, drives a stepper motor that sets the scattering angle position of the electron energy analyzer, and controls the energy ramp of the electron energy analyzer. The experimental energy loss spectra acquired by the multi-channel scaling program are analyzed by a separate software that employs a multi-Gaussian instrumental line-profile unfolding technique to fit the energy loss spectra [34].

Krypton energy loss spectra were acquired at E_0 values of 11.5 eV, 12.0 eV, 13.5 eV, 15.0 eV, and 20.0 eV for θ ranging from 15° to 130° with a typical energy resolution of around 35–45 meV for an incident current of about 13 nA to 22 nA. E_0 was calibrated using the He⁻ 2²S resonance at 19.366 eV at $\theta = 90^{\circ}$ [35,36] to obtain an E_0 with an accuracy of 50 meV or better during the entire run at that E_0 value. The CSUF spectrometer and the earlier spectrometer in [18] differ somewhat in that the former used real apertures in the analyzer as opposed to virtual apertures in the latter. Additionally, the CSUF spectrometer employs an aperture gas target collimation system rather than the earlier hypodermic needle gas collimator. In this experiment, the moveable gas source was kept fixed because the system was not observing elastic scattering as it did in previous work [37] in which elastic background scattering from surfaces was found to be significant. This

Atoms 2021, 9, 61 6 of 14

was also conducted to improve the acquired scattering counts (more acquisition time for inelastic measurements), and thus minimize statistical errors.

An important consideration in this experiment was to control the transmission efficiency for the different features (features one to four in Figure 1), which had respective energy loss values of 9.915 eV, 10.033 eV, 10.563 eV, and 10.644 eV. At small E_0 values, the residual energies of the scattered electrons become significantly different across the energy loss spectrum. Table 2 shows the ratio $\Delta E_R / E_{\bar{R}}$ (= α) at different E_0 values for the four ratios, where, e.g., in the case of r, features one and three, $\Delta E_R = E_R(1) - E_R(3)$ is the difference between the residual energies of scattered electrons having excited features one and three, and $E_R = ([E_R(1) + E_R(3)]/2)$ is the mean residual energy of these features. The parameter α indicates whether the transmission efficiency is approximately a linear function of E_R , i.e., the approximate value of the *fractional* difference in the transmission of electrons for the features involved. At $E_0 = 11.5$ eV, for example, r and r' have relative fractional transmission differences of nearly 50% while that of r'' and r''' is only \approx 2%. This means that the measured ratios $r^{\prime\prime}$ and $r^{\prime\prime\prime}$ are significantly more precise as benchmarks than r and r'. In order to circumvent this transmission problem, the scattered electron detector analyzer was first tuned to the average mid-residual energy of the features one and three or two and four, which are similar for both r and r' at any E_0 value. This employed tuning the gun and analyzer to the elastic scattering at 90° at $E_0 = E_{\bar{R}}$ before setting up the electron gun to deliver a focused beam at E_0 . At a working E_0 of 13.5 eV, for instance, the analyzer was tuned to elastically scattered electrons at $E_0 = (3.314 + 3.325)/2 \text{ eV} = 3.320 \text{ eV}$ (see Table 2). As a result, the transmission peaked at the mid- E_L of the states one and three or two and four, while it fell equally at E_L values of the features on either side of this maximum, thus giving consistently reproducible and accurate r and r' values by breaking away from a skewed transmission function for the r and r' features. This procedure does not affect r'' and r''', which were always well reproduced for any tuning conditions of the analyzer. At $E_0 \ge 15$ eV, this problem is diminished, and the r and r' ratios were found to be reproducible in the \approx 10–12% region.

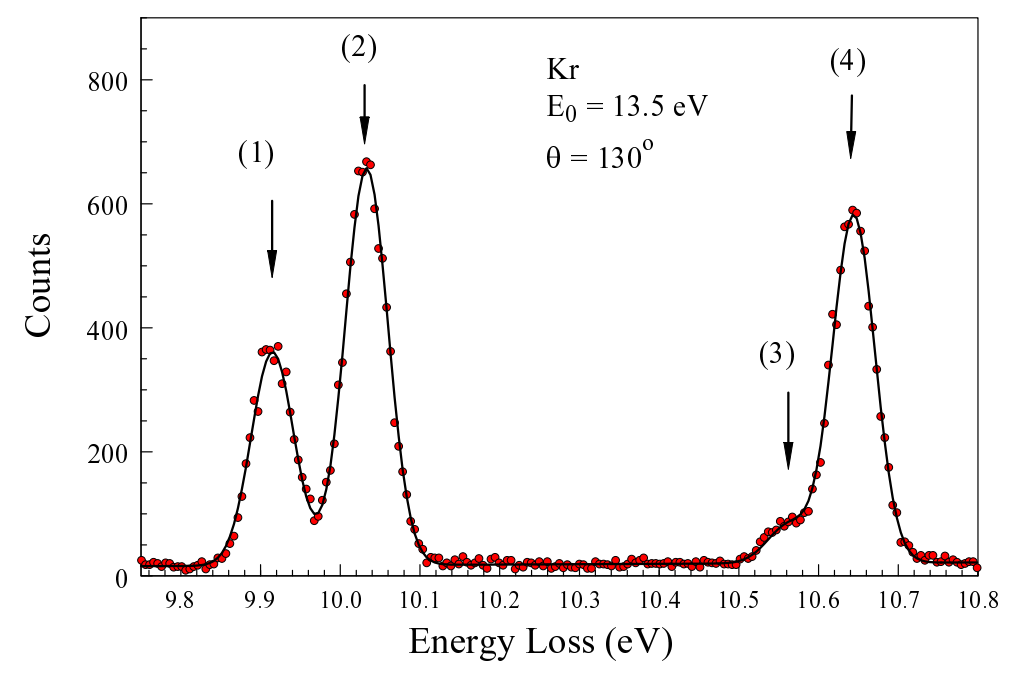


Figure 1. Electron energy loss spectrum of Kr taken at $E_0 = 13.5$ eV and $\theta = 130^\circ$. The data are the red dots, and the line is a linear least squares fit using a multi-Gaussian instrumental line profile centered at the empirical E_L values given by Moore [10] and also listed in Table 2. The features m = 1-4 are discussed in the text following Equations (1)–(4).

Atoms 2021, 9, 61 7 of 14

Table 2. Transmission parameters that affect the ratios r, r', r'', and r'''. The E_L values, listed in decreasing order for the $5s[3/2]_2$, $5s[3/2]_1$, $5s'[1/2]_0$, and $5s'[1/2]_1$ states, are taken from the recommended values of Moore [10]. See text for a detailed discussion.

$E_0 \text{ (eV)} \rightarrow$	11.5	12.0	13.5	15.0	20.0		
E_L (eV) \downarrow		E_R (e	eV) ↓				
9.876	1.624	2.124	3.624	5.124	10.124		
9.969	1.531	2.031	3.531	5.031	10.031		
10.495	1.005	1.505	3.005	4.505	9.505		
10.566	0.934	1.434	2.934	4.434	9.434		
	$\Delta E_R/E_{ar{R}}\downarrow$						
r	0.470901	0.341141	0.186755	0.12857	0.06307		
$\mathbf{r'}$	0.484381	0.344589	0.184687	0.126149	0.061341		
$\mathbf{r''}$	0.014739	0.011191	0.006499	0.004579	0.002307		
r'''	0.018308	0.012079	0.005977	0.003971	0.001874		

5. Results and Discussion

Tables 3–7 list the ratios r, r', r'', and r''' at different E_0 values. Figures 2–5 exhibit the ratios from the current measurements compared to our past ratios of Guo et al. [18] and to the DBSR-31 results. These figures will be discussed in detail below.

Figure 2 shows our present r values at several E₀ values compared to our previous measurements of this parameter and theory. We observe excellent agreement for all E_0 values with our earlier r values [18], as well as with the DBSR-31 predictions. We emphasize that the present data have significantly smaller uncertainties than our earlier measurements [18]. This is due to the better statistical counts in the present work that focused only on the lowest four excited states of Kr rather than an extended spectrum obtained before [18,19]. At our lowest E_0 of 12.0 eV, \approx 1.5 eV above threshold, we observed large deviations from the statistical ratio value of five, with values exceeding 12 (the theoretical prediction is \approx 20) at $\theta \approx 130^{\circ}$. This effect is most likely due to the markedly different residual energies of the scattered electron after exciting the $5s[3/2]_2$ state ($E_R = 2.124 \text{ eV}$) compared to the $5s'[1/2]_0$ excitation with a relatively much smaller E_R of 1.505 eV; see Table 2. The other (likely less important) factor is the presence of spin-orbit interaction in the continuum electron channel. These triplet states are well LS-coupled (cf. Table 1). Even in multi-configuration expansions, both LS-coupling and the 4p⁵6s configuration dominate, and the coupling coefficients are very close to unity for these triplet states. Our data for r deviate from five for $\theta > 0^{\circ}$ in an oscillatory manner but converge to $r \approx 5$ when $\theta \to 0^{\circ}$, except at our lowest E_0 of 12.0 eV. This effect, which is observed at all E_0 values of 13.5 eV and above, is at the 20% level for the present E_0 values.

Figure 3 exhibits our present r' values at several E_0 values. Once again, we note generally very good agreement with the earlier experimental and the theoretical predictions, except at $E_0=12.0$ eV where we see a somewhat different angular distribution for the present r' data, which are $\approx 50\%$ smaller than the earlier values of [18] and $\approx 30-50\%$ smaller than the DBSR-31 predictions for $\theta \geq 30^\circ$. This is not due to transmission effects, as can be argued on the basis of our r values, which have essentially the same instrumental transmission dependence (compared with Table 2) of ≈ 0.48 . We did not observe the oscillatory behavior predicted by theory, and the earlier values [18] are scattered at small and large θ . At $E_0=13.5$ eV, the agreement improves considerably. It is excellent at large θ but poorer at $\theta \leq 50^\circ$. The oscillatory behavior of r' at this energy is reproduced by all measured and theoretical values. At $E_0=15.0$ eV, the agreement between experiment and theory is excellent, and the oscillatory angular behavior of r' is observed in all three data sets. At $E_0=20.0$ eV, the agreement between experiments is excellent, but the measured values are significantly (by $\approx 20\%$) below theory. Here, one should expect transmission effects to

Atoms 2021, 9, 61 8 of 14

be small (see Table 2), in the region of a few percent. Nevertheless, the agreement between experiment and theory for such a difficult target is very good and certainly encouraging.

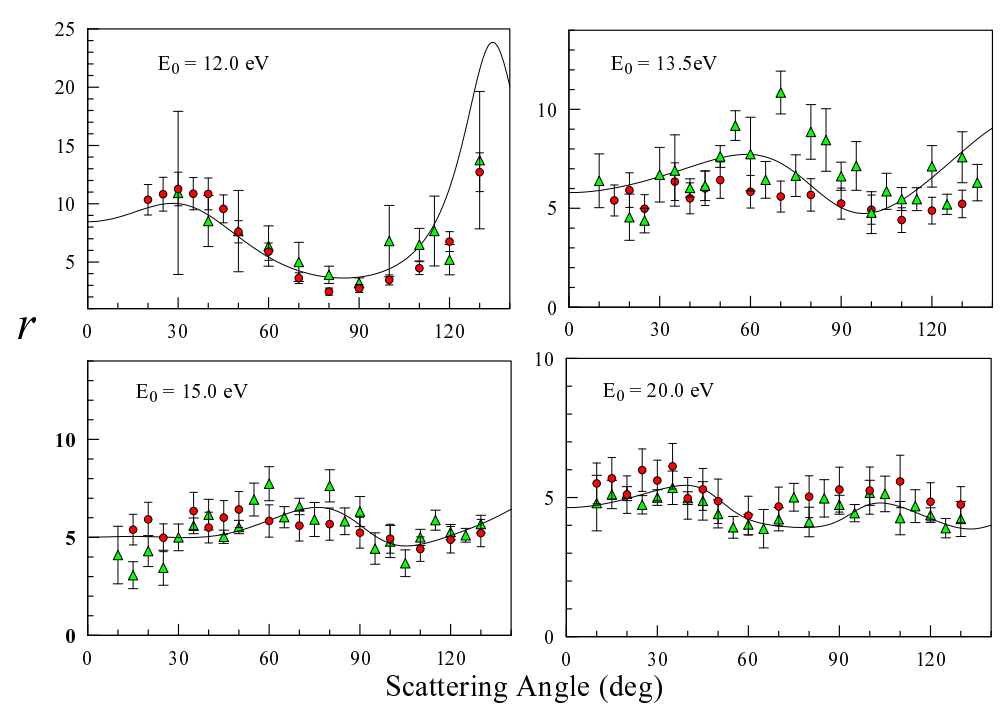


Figure 2. Ratio r for various E_0 values as a function of θ ; (•) present experimental work; (•) past experimental work of Guo et al. [18]; (—), DSBR-31 calculation.

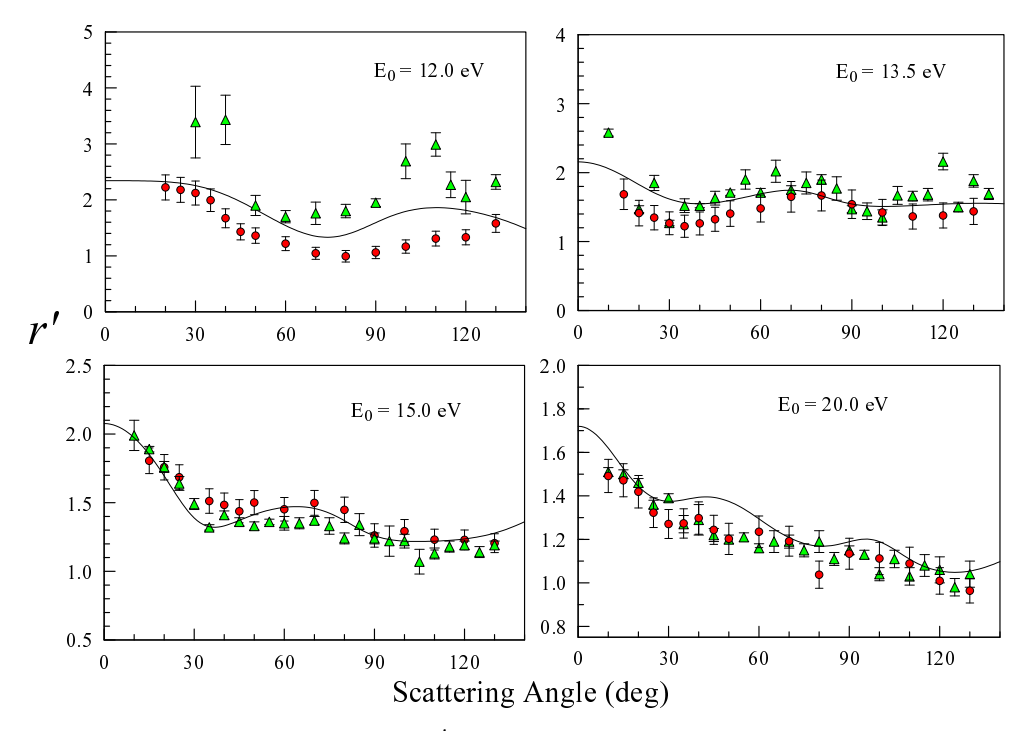


Figure 3. Same as Figure 2 but for the r' ratio.

As expected, we observe a trend of $r' \approx 1.2 = (0.74/0.67)^2$ (see Table 1), which is based on the fact that excitation of the singlet part of the wave function for the two states will ultimately dominate that of the triplet part. However, given that this limit is approached better at large than at small angles suggests that spin-dependent effects are

Atoms 2021, 9, 61 9 of 14

still important. While the trend is best for 20 eV, this is not a sufficiently high energy to predict the ratio using such a simple argument.

Table 3. Ratio r'' for Kr taken at $E_0 = 11.5$ eV, with one standard deviation uncertainty. See text for discussion.

θ (°)	r''	Err
20	0.238	0.018
25	0.242	0.019
30	0.195	0.015
35	0.174	0.014
40	0.255	0.020
45	0.290	0.023
50	0.359	0.028
60	0.679	0.053
70	1.25	0.10
80	2.37	0.19
90	2.66	0.22
100	1.70	0.10
110	0.970	0.055
120	0.520	0.030
130	0.370	0.019

Table 4. Ratios r, r', r'', and r''' for Kr taken at $E_0 = 12.0$ eV with one standard deviation error. See text for discussion.

θ (°)	r	Err	r'	Err	r''	Err	r'''	Err
20	10.3	1.3	2.22	0.22	0.383	0.039	0.082	0.009
25	10.8	1.5	2.18	0.22	0.492	0.050	0.099	0.012
30	11.3	1.4	2.12	0.21	0.507	0.051	0.096	0.010
35	10.9	1.4	2.00	0.20	0.485	0.049	0.088	0.010
40	10.8	1.4	1.67	0.17	0.592	0.060	0.091	0.010
45	9.56	1.20	1.43	0.14	0.645	0.065	0.096	0.010
50	7.59	0.95	1.36	0.14	0.665	0.067	0.119	0.013
60	5.89	0.74	1.22	0.12	0.782	0.080	0.162	0.017
70	3.62	0.45	1.04	0.11	0.973	0.100	0.281	0.030
80	2.46	0.31	0.994	0.103	1.13	0.12	0.458	0.048
90	2.73	0.34	1.06	0.11	1.08	0.11	0.420	0.044
100	3.46	0.43	1.17	0.12	0.93	0.09	0.314	0.033
110	4.47	0.56	1.31	0.13	0.76	0.08	0.224	0.023
120	6.75	0.85	1.33	0.13	0.65	0.07	0.129	0.014
130	12.7	1.7	1.58	0.16	0.54	0.06	0.068	0.008

Figure 4 presents our results for the r'' ratio, which is our most extensive ratio spanning from threshold of \approx 1.5 eV exit energy up to 10 eV (see Table 2). Since transmission for both states is the same, the reproducible characteristics of r'' is excellent and not influenced by different spectrometer detector tunings. This makes this accurate ratio a very useful parameter for testing theory. This ratio compares the LS-coupled triplet state $5s[3/2]_2$ to the $5s[3/2]_1$ mixed singlet-triplet state. At $E_0=11.5$ eV, we see excellent agreement between the present work and theory, except that the angular dependence is shifted between theory and experiment by a small amount of \approx 2°. Our r'' values are also quantitatively smaller by \approx 7%, which is within the uncertainty of the measurements. We note (not shown) that the theoretical DCS for the well LS-coupled $5s[3/2]_2$ state, which is only excitable by spin-exchange, is essentially constant in the θ range from 60° to 120° . Thus, it is the decrease in the excitation of the $5s[3/2]_1$ state that results in the rise of r''. Furthermore, we see

Atoms 2021, 9, 61 10 of 14

that at small $\theta \le 30^{\circ}$ rises. As discussed for r' above, this result supports the remaining importance of spin-exchange processes at small θ for the energies investigated in this study.

Table 5. Same as Tab	ble 4 but for $E_0 =$	13.5 eV. See text	for discussion.
-----------------------------	-----------------------	-------------------	-----------------

θ (°)	r	Err	r'	Err	r''	Err	r'''	Err
15	5.49	0.99	1.69	0.22	0.111	0.012	0.034	0.004
20	4.95	0.80	1.41	0.18	0.172	0.017	0.049	0.005
25	5.65	0.93	1.35	0.18	0.253	0.026	0.061	0.006
30	5.56	0.91	1.26	0.17	0.339	0.034	0.078	0.008
35	6.14	1.01	1.22	0.16	0.418	0.043	0.083	0.009
40	6.14	1.00	1.26	0.17	0.478	0.049	0.099	0.010
45	7.80	1.30	1.32	0.17	0.513	0.052	0.087	0.009
50	7.50	1.24	1.41	0.19	0.514	0.052	0.097	0.011
60	8.28	1.38	1.48	0.20	0.591	0.060	0.107	0.012
70	8.15	1.43	1.649	0.223	0.66	0.07	0.134	0.016
80	7.54	1.29	1.67	0.22	0.70	0.07	0.156	0.018
90	6.04	1.02	1.54	0.21	0.69	0.07	0.176	0.020
100	4.98	0.83	1.42	0.19	0.57	0.06	0.164	0.018
110	4.84	0.80	1.36	0.18	0.53	0.05	0.149	0.016
120	5.87	0.97	1.38	0.18	0.54	0.06	0.127	0.014
130	6.8	1.1	1.44	0.19	0.53	0.05	0.111	0.012

Table 6. Same as Table 4 but for $E_0 = 15.0$ eV. See text for discussion.

θ (°)	r	Err	r'	Err	r''	Err	r'''	Err
15	5.40	0.78	1.81	0.09	0.058	0.006	0.019	0.002
20	5.92	0.87	1.76	0.09	0.097	0.010	0.029	0.004
25	4.98	0.71	1.69	0.09	0.160	0.017	0.054	0.007
35	6.35	0.95	1.51	0.09	0.347	0.037	0.083	0.011
40	5.50	0.78	1.48	0.09	0.404	0.043	0.109	0.014
45	6.01	0.87	1.44	0.08	0.404	0.043	0.097	0.012
50	6.42	0.92	1.50	0.09	0.446	0.047	0.105	0.013
60	5.84	0.82	1.45	0.09	0.510	0.054	0.130	0.016
70	5.60	0.78	1.50	0.09	0.577	0.061	0.154	0.019
80	5.68	0.82	1.45	0.09	0.659	0.071	0.169	0.022
90	5.24	0.79	1.26	0.09	0.703	0.078	0.170	0.023
100	4.93	0.74	1.29	0.08	0.581	0.064	0.155	0.020
110	4.40	0.62	1.23	0.08	0.553	0.060	0.155	0.019
120	4.88	0.67	1.23	0.07	0.539	0.057	0.136	0.016
130	5.22	0.70	1.21	0.07	0.620	0.065	0.142	0.016

Our findings might also help to interpret the reversal of the angular momentum perpendicular to the scattering plane, (L_{\perp}) , imparted to the target. This was found at similarly small θ in the excitation of the resonance transition in Ne [38], i.e., of the $2p^53s[3/2]_1$ LS-coupled 1P_1 component, which is again mixed (but to a lesser extent) with the LS-coupled 3P_1 component. It is the latter's excitation via spin-exchange that could enable a physical explanation for the reversal of L_{\perp} compared to the case for a direct singlet \rightarrow singlet excitation.

At $E_0 = 12.0$ eV, the theory shows excellent agreement with experiment, but at E_0 of 13.5 eV and 15.0 eV it predicts a clear rise at $\theta \approx 80^\circ$. This is again likely due to a drop in the direct excitation process of the $5s[3/2]_1$ state, which in turn is due to an effective overestimate of the singlet LS-contribution as aforementioned for r'. The feature in r'' that peaks around $\theta = 30^\circ$ for $E_0 = 20.0$ eV is found to be in excellent agreement between both experiments and theory. At this energy, however, the theory predicts oscillations that are

Atoms 2021, 9, 61 11 of 14

not visible to the same extent in the measurements. Overall, we again judge the agreement between experiment and theory as encouragingly good.

Table 7. Same as	Table 4 but for	$E_0 = 20.0 \text{ eV}$.	See text for a	discussion.
-------------------------	-----------------	---------------------------	----------------	-------------

θ (°)	r	Err	r'	Err	r''	Err	r'''	Err
10	5.51	0.73	1.49	0.08	0.086	0.009	0.023	0.003
15	5.69	0.75	1.47	0.08	0.146	0.015	0.038	0.004
20	5.10	0.67	1.42	0.07	0.225	0.023	0.062	0.007
25	5.98	0.76	1.32	0.07	0.278	0.028	0.061	0.007
30	5.61	0.73	1.27	0.07	0.290	0.030	0.066	0.007
35	6.12	0.82	1.27	0.07	0.264	0.027	0.055	0.006
40	4.97	0.75	1.30	0.07	0.237	0.026	0.062	0.008
45	5.29	0.75	1.24	0.07	0.194	0.020	0.046	0.006
50	4.87	0.80	1.20	0.07	0.196	0.022	0.050	0.007
60	4.35	0.70	1.23	0.07	0.201	0.023	0.057	0.008
70	4.68	0.69	1.19	0.07	0.259	0.028	0.066	0.009
80	5.03	0.75	1.04	0.06	0.387	0.042	0.080	0.011
90	5.28	0.81	1.13	0.07	0.452	0.050	0.097	0.013
100	5.25	0.85	1.11	0.07	0.471	0.054	0.102	0.015
110	5.58	0.94	1.09	0.08	0.513	0.059	0.100	0.015
120	4.85	0.69	1.01	0.06	0.581	0.062	0.121	0.015
130	4.74	0.65	0.964	0.056	0.624	0.066	0.128	0.015

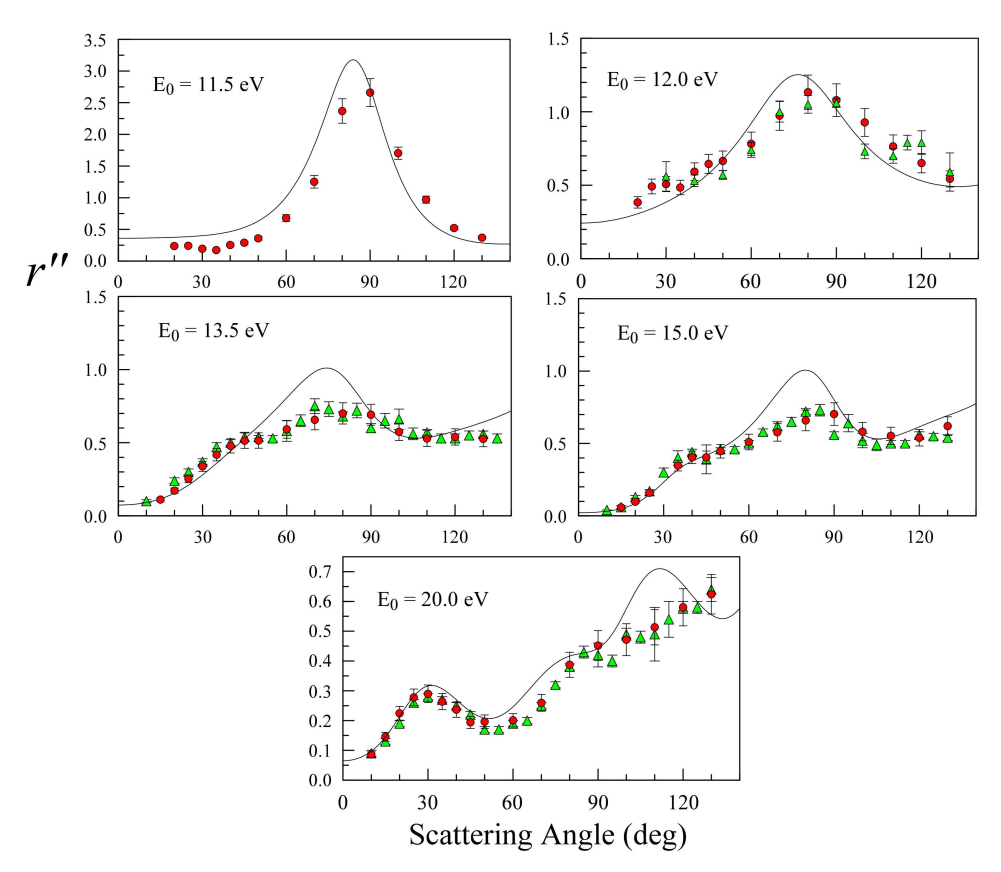


Figure 4. Same as Figure 2 but for the r'' ratio.

For the r''' ratio, exhibited in Figure 5, we observe a similar behavior as for r''. At $E_0 = 12.0$ eV, the agreement with theory is excellent. The earlier measurements show much more scatter because the DCS (thus the scattering intensity) of the $5s'[1/2]_0$ state is the smallest of the four features (see also Figure 2). At small θ , we observe a similar rise in

Atoms 2021, 9, 61 12 of 14

r''' as for r'', which is an indication that spin exchange processes are prevalent at these angles. At $E_0=13.5$ eV, we again note the increased r'' values at the mid-angles around 80° as well as non-zero r''' values for $\theta \to 0^{\circ}$, similarly as for 12.0 eV. This indicates that small-angle spin-exchange processes exist in this system. At $E_0=15.0$ eV, the overall agreement is excellent, except for the "bump" in r'' at mid-angles around 80° . At 20.0 eV, a similar oscillatory behavior in r''' as for r'' is observed, with some disagreement between experiment and theory for $\theta \geq 50^{\circ}$. We note again that the feature peaking at $\theta=30^{\circ}$ (as in r'' at this E_0) is in excellent agreement between both experimental datasets and the DBSR-31 predictions, although somewhat less pronounced compared to r''. Clearly, the overall agreement with theory is encouragingly good for this complex target.

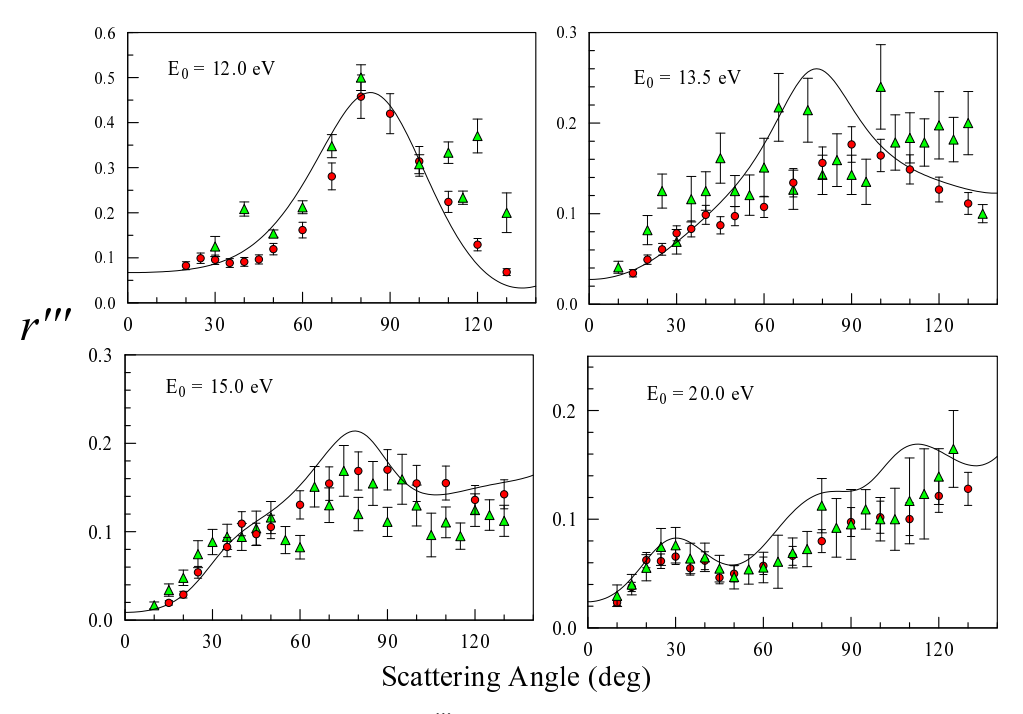


Figure 5. Same as Figure 2 but for the r''' ratio.

6. Conclusions

New and improved measurements of the intensity ratios r, r', r'', and an additional useful ratio r''' for the first four excited states of Kr were presented and compared to earlier ratios taken in our laboratory [18] and compared to benchmark DBSR calculations. The agreement between the measurements is very good for r and r' and excellent for r'' and r'''. This provides confidence in their overall reliability. The overall agreement with the theoretical predictions is also very good to excellent, but it suggests places where the DBSR model may need to be improved even further.

Similar measurements of ratios will soon be carried out for Xe to further extend the tests of the DBSR results published in [32]. Depending on the outcome, new calculations with a further improved target structure and even more coupled states in the collision part of the problem may be necessary. We hope that the present work on Kr and the planned experiment on Xe will provide an impetus for the theory to further push benchmark calculations for electron scattering from multi-electron targets with more than two electrons outside of a structureless core.

Author Contributions: The project was conceived by M.A.K. who also supervised the experimental part of the study carried out by A.S. and J.-B.F. The calculations were carried out by O.I.Z. and K.B. The manuscript was mostly prepared by M.A.K. and K.B. All authors have read and agreed to the published version of the manuscript.

Atoms 2021, 9, 61 13 of 14

Funding: This work was funded by the US National Science Foundation under Grant No. NSF-RUI AMO 1911702 (MAK), which included a post-doctoral fellowship for A. Sakaamini. The work of OZ and KB was supported by the NSF under grant Nos. PHY-1803844, OAC-1834740, PHY-2110023, and the XSEDE allocation TG-PHY-090031.

Institutional Review Board Statement: Not applicable.

Informed Consent Statement: Not applicable.

Data Availability Statement: Not applicable.

Conflicts of Interest: The authors declare no conflict of interest. The funders had no role in the design of the study; in the collection, analyses, or interpretation of data; in the writing of the manuscript or in the decision to publish the results.

Sample Availability: Tabulated results of the cross sections in digital form are available from the authors upon request.

Abbreviations

The following abbreviations are used in this manuscript:

DCS Angle-differential cross section;

DBSR Dirac B-Spline R-matrix.

References

1. Murphy, A.B.; Tam, E. Thermodynamic properties and transport coefficients of arc lamp plasmas: Argon, krypton and xenon. *J. Phys. D Appl. Phys.* **2014**, *47*, 295202. [CrossRef]

- 2. Kawanaka, J.; Shirai, T.; Kubodera, S.; Sasaki, W. 1.5 kW high-peak-power vacuum ultraviolet flash lamp using a pulsed silent discharge of krypton gas. *Appl. Phys. Lett.* **2001**, *79*, 3752. [CrossRef]
- 3. Obenschain, S.; Lehmberg, R.; Kehne, D.; Hegeler, F.; Wolford, M.; Sethian, J.; Weaver, J.; Karasik, M. High-energy krypton fluoride lasers for inertial fusion. *Appl. Opt.* **2001**, *54*, F103. [CrossRef]
- 4. Guo, X.; Trajmar, S.; Zeman, V.; Bartschat, K.; Fontes, C.J. Low-energy electron impact excitation cross sections for the 4p⁵5s levels of krypton—Supplementary test of collisions models for the heavy rare gases. *J. Phys. B At. Mol. Opt. Phys.* **1999**, 32, L155. [CrossRef]
- 5. Bartschat, K.; Madison, D.H. Electron impact excitation of rare gases: Differential cross sections and angular correlation parameters for neon, argon, krypton and xenon. *J. Phys. B At. Mol. Phys.* **1987**, 20, 5839. [CrossRef]
- 6. Furness, J.B.; McCarthy, I.E. Semiphenomenological optical model for electron scattering on atoms. *J. Phys. B At. Mol. Phys.* **1973**, 6, 2280. [CrossRef]
- 7. Zuo, T.; McEachran, R.P.; Stauffer, A.D. Relativistic distorted-wave calculation of electron excitation of heavy noble gases. *J. Phys. B At. Mol. Opt. Phys.* **1992**, 25, 3393. [CrossRef]
- 8. Cowan, R.D. The Theory of Atomic Structure and Spectra; University of California Academic Press: Riverside, CA, USA, 1981.
- 9. Fontes, C.J.; Los Alamos National Laboratory, Los Alamos, NM, USA. Personal communication, 1996.
- 10. Moore, C.E. Atomic Energy Levels; NSRDS-NBS Publication; US Govt Publishing: Washington, DC, USA, 1957; Volume 35.
- 11. Bray, I.; Stelbovics, A.T. Convergent close-coupling calculations of electron-hydrogen scattering. *Phys. Rev. A* **1992**, *46*, 6995. [CrossRef]
- 12. Fursa, D.V.; Bray, I. Calculation of electron-helium scattering. Phys. Rev. A 1995, 52, 1279. [CrossRef]
- 13. Bartschat, K.; Hudson, E.T.; Scott, M.P.; Burke, P.G.; Burke, V.M. Electron—Atom scattering at low and intermediate energies using a pseudo-state/R-matrix basis. *J. Phys. B At. Mol. Phys.* **1996**, 29, 115. [CrossRef]
- 14. Hudson, E.T.; Bartschat, K.; Scott, M.P.; Burke, P.G.; Burke, V.M. Electron scattering from helium atoms. Phase shifts, resonance parameters and total cross sections. *J. Phys. B At. Mol. Opt. Phys.* **1996**, 29, 5513. [CrossRef]
- 15. Zammit, M.C.; Savage, J.S.; Fursa, D.V.; Bray, I. Complete solution of electronic excitation and ionization in electron-hydrogen molecule scattering. *Phys. Rev. Lett.* **2016**, *116*, 233201. [CrossRef]
- 16. Khakoo, M.A.; Trajmar, S.; LeClair, L.R.; Kanik, I.; Csanak, G.; Fontes, C.J. Differential cross sections for electron impact excitation of Xe: I. Excitation of the five lowest levels; experiment and theory. *J. Phys. B At. Mol. Opt. Phys.* **1996**, 29, 3455. [CrossRef]
- 17. Khakoo, M.A.; Trajmar, S.; Wang, S.; Kanik, I.; Aguirre, A.; Fontes, C.J.; Clark, R.E.H.; Abdallah, J. Differential cross sections for electron impact excitation of Xe: II. Excitation of the sixth to twentieth lowest levels; experiment and theory. *J. Phys. B At. Mol. Opt. Phys.* **1996**, 29, 3477. [CrossRef]
- 18. Guo, X.; Mathews, D.F.; Mikaelian, G.; Khakoo, M.A.; Crowe, A.; Kanik, I.; Trajmar, S.; Zeman, V.; Bartschat, K.; Fontes, C.J. Journal of Physics B: Atomic, Molecular and Optical Physics Differential cross sections for electron-impact excitation of krypton at low incident energies: I. Excitation of the 4p⁵5s configuration. *J. Phys. B At. Mol. Opt. Phys.* **2000**, *33*, 1895. [CrossRef]

Atoms 2021, 9, 61 14 of 14

19. Guo, X.; Mathews, D.F.; Mikaelian, G.; Khakoo, M.A.; Crowe, A.; Kanik, I.; Trajmar, S.; Zeman, V.; Bartschat, K.; Fontes, C.J. Journal of Physics B: Atomic, Molecular and Optical Physics Differential cross sections for electron-impact excitation of krypton at low incident energies: II. Excitation of the 4p⁵5p, 4p⁵4d and 4p⁵56s configurations. *J. Phys. B At. Mol. Opt. Phys.* **2000**, 33, 1921. [CrossRef]

- 20. Berrington, K.A.; Eissner, W.; Norrington, P.H. RMATRX1: Belfast atomic R-matrix codes. *Comp. Phys. Commun.* **1995**, 92, 290. [CrossRef]
- 21. Zatsarinny, O. BSR: B-Spline Atomic R-Matrix Codes. Comp. Phys. Commun. 2006, 174, 273. [CrossRef]
- 22. Zatsarinny, O.; Bartschat, K. XXVIII International Conference on Photonic, Electronic and Atomic Collisions (ICPEAC 2013) IOP Publishing. *J. Phys. Conf. Ser.* **2014**, *488*, 012044. [CrossRef]
- Zatsarinny, O.; Bartschat, K. Relativistic B-spline R-matrix method for electron collisions with atoms and ions: Application to low energy electron scattering from Cs. Phys. Rev. A 2008, 77, 062701. [CrossRef]
- 24. Oleg Zatsarinny's GitHub Repository. Available online: https://github.com/zatsaroi (accessed on 1 August 2021).
- 25. Zatsarinny, O.; Wang, Y.; Bartschat, K. Electron-impact excitation of argon at intermediate energies. *Phys. Rev. A* **2014**, *89*, 022706. [CrossRef]
- Brunger, M.J.; Buckman, S.J. Electron–molecule scattering cross-sections. I. Experimental techniques and data for diatomic molecules. *Phys. Rep.* 2002, 357, 215. [CrossRef]
- 27. Zawadzki, M.; Wright, R.; Dolmat, G.; Martin, M.F.; Hargreaves, L.; Fursa, D.V.; Zammit, M.C.; Scarlett, L.H.; Tapley, J.K.; Savage, J.S.; et al. Time-of-flight electron scattering from molecular hydrogen: Benchmark cross sections for excitation of the $X^1\Sigma_g^+ \to b^3\Sigma_u^+$ transition. *Phys. Rev. A* **2018**, *97*, 050702(R). [CrossRef]
- 28. Muse, J.; Silva, H.; Lopes, M.C.A.; Khakoo, M.A. Low energy elastic scattering of electrons from H₂ and N₂. *J. Phys. B At. Mol. Opt. Phys.* **2008**, 41, 095203. [CrossRef]
- 29. Khakoo, M.A.; Wrkich, J.; Larsen, M.; Kleiban, G.; Kanik, I.; Trajmar, S.; Brunger, M.J.; Teubner, P.J.O.; Crowe, A.; Fontes, C.J.; et al. Differential cross sections and cross-section ratios for electron-impact excitation of the neon 2p⁵3s configuration. *Phys. Rev. A* **2002**, *65*, 062711. [CrossRef]
- 30. Bartschat, K.; Madison, D.H. Non-statistical branching ratios for excitation of the $(np^5(n+1)s)^{1,3}P_{0,1,2}$ states in noble gases. *J. Phys. B At. Mol. Opt. Phys.* **1992**, 25, 4619. [CrossRef]
- 31. Zatsarinny, O.; Bartschat, K. Electron impact excitation of neon at intermediate energies. Phys. Rev. A 2012, 86, 022717. [CrossRef]
- 32. Zatsarinny, O.; Bartschat, K. Benchmark calculations for near-threshold electron-impact excitation of krypton and xenon atoms. *J. Phys. B At. Mol. Opt. Phys.* **2010**, 43, 074031. [CrossRef]
- 33. Jönsson, P.; He, X.; Froese Fischer, C.; Grant, I.P. The grasp2K relativistic atomic structure package. *Comp. Phys. Commun.* **2007**, 177, 597–622. [CrossRef]
- 34. Khakoo, M.A.; Beckmann, C.E.; Trajmar, S.; Csanak, G. Electron-impact excitation of the $ns[3/2]^o$ and $n[1/2]^o$ levels of Ne, Ar, Kr and Xe. *J. Phys. B At. Mol. Opt. Phys.* **1994**, 27, 3159. [CrossRef]
- 35. Brunt, J.H.; King, G.C.; Read, F.H. Resonance structure in elastic electron scattering from helium, neon and argon. *J. Phys. B At. Mol. Phys.* **1977**, *10*, 1289. [CrossRef]
- 36. Gopalan, A.; Bömmels, J.; Götte, S.; Landwehr, A.; Franz, K.; Ruf, M.W.; Hotop, H.; Bartschat, K. A novel electron scattering apparatus combining a laser photoelectron source and a triply differentially pumped supersonic beam target: Characterization and results for the He⁻(1s2s²) resonance. *Eur. Phys. J. D* 2002, 22, 17. [CrossRef]
- 37. Khakoo, M.A.; Keane, K.; Campbell, C.; Guzman, N.; Hazlett, K. Low energy elastic electron scattering from ethylene. *J. Phys. B At. Mol. Opt. Phys.* **2007**, *40*, 3601. [CrossRef]
- 38. Hargreaves, L.R.; Campbell, C.; Khakoo, M.A.; Zatsarinny, O.; Bartschat, K. Unusual angular momentum transfer in electron-impact excitation of neon. *Phys. Rev. A* **2012**, *85*, 050701(R). [CrossRef]